

Investigation and Development of high strength AA2024-AA7075 aluminium alloys sheets studies their mechanical and microstructural behaviour by friction stir welding

M. DINESH¹ and G. VENU MADHAV

Department of Mechanical Engineering Raghu Institute of Technology, Visakhapatnam (Affiliated To JNT University, Kakinada, A.P) dineshdinumudedla@gmail.com

Abstract

The aim of the present work is to investigate on the mechanical and microstructural properties of dissimilar AA2024 and AA7075 aluminium sheets joined by friction stir welding (FSW) and under water friction stir welding. The two sheets, aligned with perpendicular rolling directions, have been successfully welded; successively, the welded sheets have been analyze the influence of rotation speed and traverse speed over the microstructural and tensile properties with respect to the parent materials. Effect of welding speed on microstructures, hardness distribution and tensile properties of the welded joints were investigated. From microstructural analysis it is evident that the material placed on the advancing side dominates the nugget region. The fracture surface of the tensile tested samples was examined using scanning electron microscope (SEM). The grain structure and second phase particles in various regions including the dynamically recrystallized zone (DXZ), thermo-mechanically affected zone (TMAZ), and heat affected zone (HAZ) of a friction stir weld aluminum alloy AA7075 were investigated and compared with the unaffected base metal. The various regions were studied in detail to better understand the microstructural evolution during friction stir welding (FSW) and under water friction stir welding.

Keywords: Under water Friction-stir welding, Dissimilar materials AA2xxx and AA7xxx, Microstructure analysis, Mechanical properties and Scanning electron microscope.

1. Introduction

Friction Stir Welding (FSW) is a solid-state joining technique invented and patented by The Welding Institute (TWI) in 1991 for butt and lap welding of ferrous and non-ferrous metals and plastics¹. Since its invention, the process has been continually improved and its scope of application expanded. FSW is a continuous process that involves plunging a portion of a specially shaped rotating tool between the butting faces of the joint. The relative motion between the tool and the substrate generates frictional heat that creates a plasticized region around the immersed portion of the tool. The shoulder prevents the plasticized material from being expelled from the weld. The tool is moved relatively along the joint line, forcing the plasticized material to coalesce behind the tool to form a solid-phase joint [1].

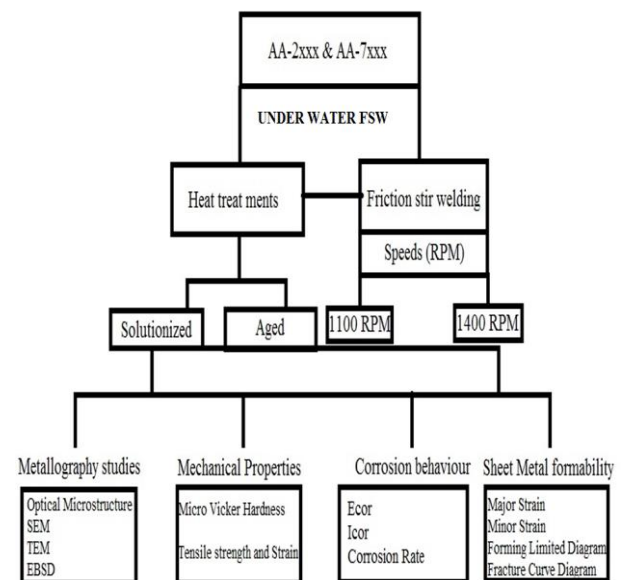
Cite this article as: M.Dinesh And G.Venu Madhav, "Investigation and Development of high strength AA2024-AA7075 aluminium alloys sheets studies their mechanical and microstructural behaviour by friction stir welding", International Journal & Magazine of Engineering, Technology, Management and Research (IJMETMR), ISSN 2348-4845, Volume 9 Issue 8, August 2022, Page 12-22.

The benefits of this technology include: low distortion, greater weld strength compared to the fusion welding process, little or no porosity, no filler metals, little or no post-weld repair, no solidification cracking, no welding fumes or gases, improved corrosion resistance, and lower cost in production applications [2-5]. Because of the many demonstrated advantages of FSW over fusion welding techniques, the commercialization of FSW is proceeding at a rapid pace. In fact, it is currently being applied in production activities that involve both large and small-scale products. Furthermore, most of the work done to bring FSW to production applications has not only been practical in nature, but has also been driven primarily by the pressing need of industries. However, the information generated through previous work is often hidden from the public for proprietary reasons. FSW of low melting temperature materials, such as aluminium and its alloys, and other similar material joining have now been commercialized in the aerospace, marine, and transportation industries and in recent years, considerable interest has been generated in joining dissimilar materials [6].

The need for joints between dissimilar materials often arises in industrial applications which are experiencing complex loading conditions. This provides the platform for the need / or the availability of a sound joining technique for dissimilar materials, because of the requirements, such as light weight and high performance. High quality joints between Aluminium (Al) and Copper (Cu) will promote the use of such joints in industrial applications especially in the field of electrical components. Aluminium (Al) and Copper

(Cu) are widely applied in engineering structures due to their unique properties, such as high electric conductivity, heat conductivity, corrosion resistance and mechanical properties [7]. Al and Cu are used in the production of bus-bars. A bus-bar is an electrical conductor that makes a common connection between several circuits; and it is found in the interconnection of the incoming and outgoing transmission lines and transformers at an electrical substation. Bus-bars are also used to connect generators and the main transformers in a power plant [8]. However, due to the inherently different chemical, mechanical and thermal properties of the materials being joined, a dissimilar joining process presents more challenges than a similar materials joining process.

1.2 Methodology



2. Experimental Procedure

Dissimilar 2024 and 7075 Al welded alloy sheets, respectively in the solutionized conditions have been produced by Friction Stir Welding as shown in Fig. 1. Both the sheets

measured 6 mm thickness. The longitudinal direction of the FSW line was perpendicular to the rolling direction of the 2024 alloy and parallel to the rolling direction of the 7075 alloy; this joint choice has been selected to simulate the most severe mechanical combination with respect to the conventional reference welding trials found in literature, in which both the sheets are welded with the same extrusion direction. The welding speed was set to 1100 RPM and 1400RPM and feed rate 2.67 mm/s, according to optimized wildings parameters determined so far; the welding tool was fixed to the rotating axle in the clockwise direction while the parts, fixed at the backside, have been translated. The tool nib was 6 mm diameter and 6 mm long; a 20 mm diameter shoulder has been machined perpendicular to the tool axis; the tilt angle of the tool was set to 3°.

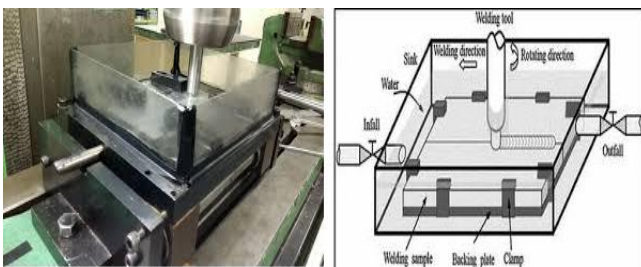


Fig 1 Dissimilar metals AA2024 and AA7075 Al welded alloy sheets with tensile sample and FSW tool.

3. Result and discussion

The present chapter discusses structure-property correlations of AA-2xxx and AA-7xxx alloy subjected to precipitation hardening behaviour. Initially, microstructural characterization of alloys was presented. Further, mechanical properties such as hardness and tensile properties were evaluated. The metallurgical properties such as crystallite size, micro strain and dislocation density were calculated by XRD and correlated with mechanical properties. The above parameters were also used in evaluating the various strengthening mechanisms contributing to the overall behaviour of precipitation hardening. AA-2xxx and AA-7xxx alloys by FSW. The experimental procedures for studying the above alloys for metallographic, mechanical and electrochemical properties analysis in the detailed manner.

3.1 Microstructure Analysis

The microstructural analyses were carried out on AA-2xxx and AA-7xxx alloy samples using Optical microscope. The micrographs shown in fig. 1 from the micrographs, the of AA-2xxx and AA 7xxx alloys ascast condition microstructures shown in the finer grains were observed with the uniform distribution of finer precipitates are observed in the sample. On other hand, the coarser grain structure is witnessed with the thick grain boundary in the side due to the temperature gradient variation throughout the sample during the casting. This is attributed by fast heat dissipation at during metal casting. The structure consists of α -Al matrix and complex intermetallics Al_6CuMg_4 , $CuAl_2$ and $MgZn_2$ and Al_2CuMg by non-equilibrium solidification. The presence of

intermetallic compounds is confirmed by X-ray diffraction studies (Fig. 2). The intermetallics are predominantly segregated along the grain boundaries which are brittle in nature and significantly affect the mechanical properties of casting. Microstructures of high alloy containing AA-2xxx and AA-7xxx series aluminium with different conditions (solutionized and aged) are shown in fig. 1. The equilibrium precipitates are dissolved in α -aluminium matrix during Solutionizing treatment. However, there are some undissolved precipitates in the matrix. The microstructure of peak aged alloy shows undissolved compounds and fine precipitates.

3.2 XRD Analysis

3.2.1. Phase Identification

XRD analysis of the as cast sample was done by a Goniometer (Ultima3theta-theta gonio, under 40kV/30mA - X-Ray, $2\theta / \theta$ – Scanning mode, Fixed Monochromator). Data was taken for the 2θ range of 10 to 80 degrees with a step of 0.02 degree. In this XRD results peaks of aluminium and intermetallics. It is evident and confirmed that a phase of lithium is appeared in XRD patterns.

The structure consists of α -Al matrix and complex intermetallics Al_6CuMg_4 , Al_4Cu_3Zn , Al_2CuMg , $MgZn_2$ and Al_2Cu by non-equilibrium solidification. The XRD patterns are similar in all these conditions and showed the presence of T (Al_6CuMg_4 and Al_4Cu_3Zn), M ($AlCuMg$ and $MgZn_2$) and S (Al_2CuMg) phases. The XRD peak of Al–Zn–Mg–Cu alloy $MgZn_2$ it is evident from the XRD profile both soluble and insoluble compounds are seen evidence of XRD as shown in fig-2.

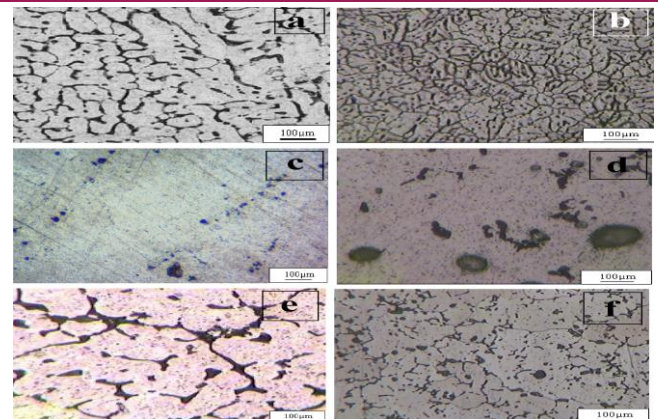


Fig. 2 Microstructure of AA-2xxx and AA-7xxx Aluminium alloys, a, b) Cast, c, d) Solutionized, e, f) Aged,

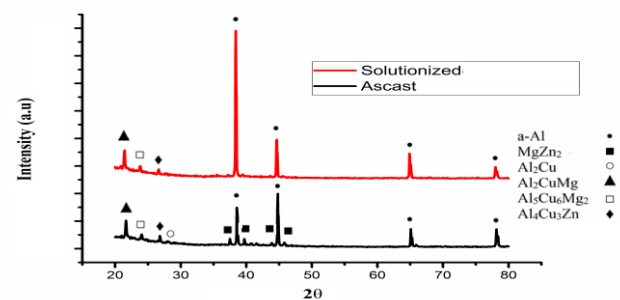


Fig. 3 X-ray diffraction patterns of AA-7xxx alloy at ascast and solutionized conditions

3.3 Mechanical Properties

3.3.1. Micro hardness

Vickers hardness values for AA-2xxx and AA-7xxx alloy in different conditions was shown in Table (1 & 2). Ascast value showed lower hardness values due to its inhomogeneous structure. Aged condition sample exhibited higher hardness values than that of solutionized condition due to increased dislocation cell structure and precipitation hardening strengthening and solutionized sample shows lower hardness comparing ascast and aged samples because of after solutionized at different temperatures and with respected time dissolves precipitates within the matrix. The comparison of micro hardness

values for the AA-2xxx and 7xxx exhibit higher hardness values of AA-7xxx material comparing AA-2xxx cause of adding elements of Zn and Mg to form the precipitates (Al_2Cu & $MgZn_2$) and second phase particle (Al_2CuMg & Al_5Cu_6Mg).

3.3.2. Tensile properties

Table: 1. Tensile properties of AA-2xxx alloy

Conditions	(Hv) _{0.3}	UTS (MPa)	%Elongation
As cast	124	280±10	5
Solutionized	102	225±10	10
Aged	140	520±10	8

Table: 2. Tensile properties of AA-7xxx alloy

Conditions	(Hv) _{0.3}	UTS (MPa)	%Elongation
As cast	148	350±10	3.8
Solutionized	120	265±10	7
Aged	165	580±10	6

Stress – strain curves of AA-2xxx and AA-7xxx alloy with different conditions are shown in fig (4. & 5). The ultimate tensile strength (UTS) of AA-2xxx alloy, cast, solutionized, aged, cold rolling, alloy is 280MPa, 225MPa, and 520MPa, the elongation is 5%, 10%, 8%, respectively (Table 1). The ultimate tensile strength (UTS) of AA-7xxx alloy, cast, solutionized, aged alloy is 350MPa, 265MPa, and 580MPa, the elongation is 3.8%, 7%, 6%, respectively (Table 2). Cast alloy has resulted good strength by solid solution and lower ductility by micro-segregation of complex intermetallics along the grain boundaries. Precipitation hardened aluminum alloy

exhibits approximately 40% increment in UTS than that of cast alloy with (6-8) % ductility. The increment in strength and ductility after ageing are attributed by combined effect of solid solution, precipitation hardening and dispersion hardening. The strength and hardness of aged alloy are better than that of cast and solutionized alloy. During solutionizing and quenching of AA-2xxx and AA-7xxx alloy, the solute atoms are getting dissolved and the internal strain from the alloy is also completely relieved. The effect of ageing temperature on structural transformation and increasing mechanical properties is not appreciated due to the strong pinning effect of insoluble compounds.

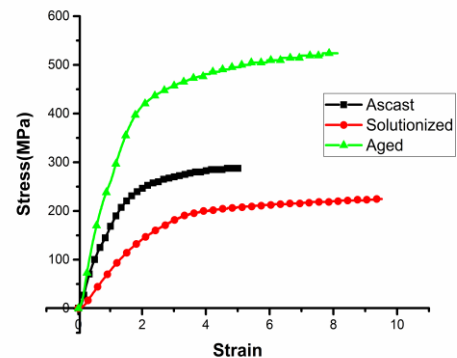


Fig. 4 Stress-strain curves of AA-2xxx alloy at different condition.

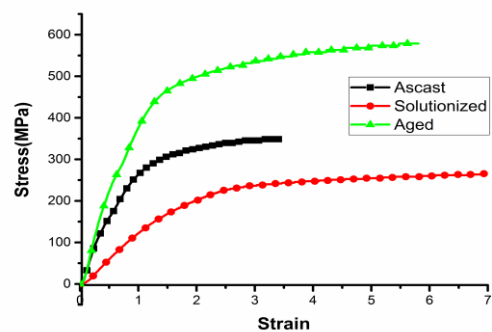


Fig. 5 Stress-strain curves of AA-7xxx alloy at different condition.

3.4 Fracture Analysis

SEM fractographs of tensile tested AA-2xxx and AA-7xxx alloy (cast, solutionized and aged) are shown in Fig. (6). Fractographs of as cast, solutionized and aged alloy show mixed mode of fracture. The dimple size is reduced in aged condition. Some regions of the fractographs exhibit well developed primary and secondary dimples; however, cleavage facets are observed in some other regions. Ultra-fine dimples are also noticed caused by the fine precipitates, mainly Al_2Cu shown in AA-2xxx and Al_2Cu , $MgZn_2$ shown in AA-7xxx.

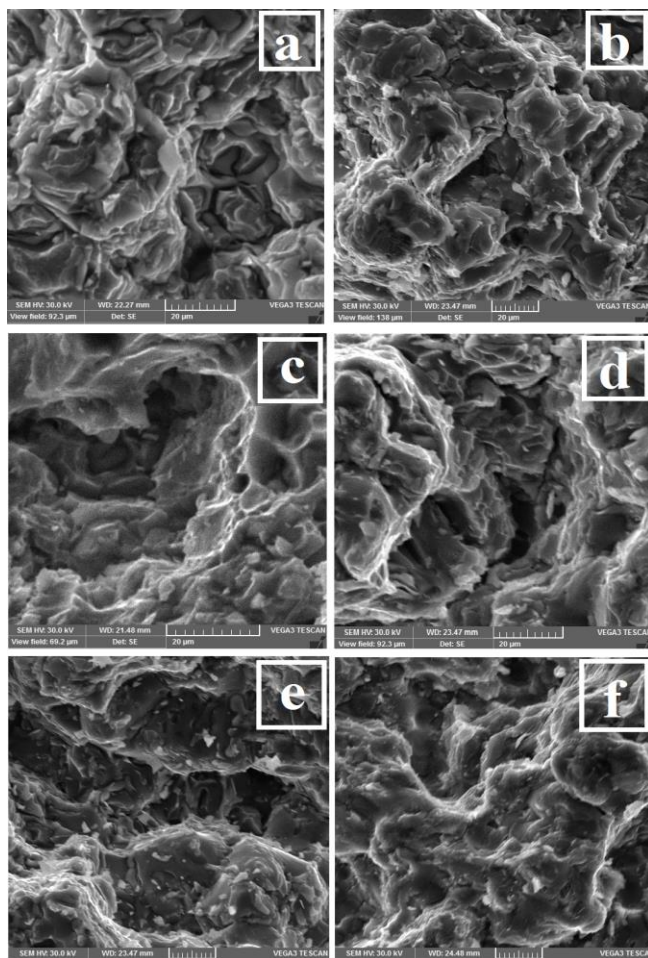


Fig. 6 Fracture surface of AA-2xxx and AA-7xxx alloys, a, b) Cast, c, d) Solutionized, e, f) Aged

3.5 FSW Microstructural Behaviour

In the present study, the dissimilar materials AA2024 and AA7075 aluminium alloys have been successfully joined with the FSW Process and no visible superficial porosity or macroscopic defects have been observed on both the top and rear welded surfaces Fig 7. Light microscopy observations have been done on the welded specimen cross-sections Fig. 7a; the FSW Process applied on dissimilar AA2024 and AA7075 aluminium alloys revealed the classical formation of the elliptical ‘onion’ structure in the centre weld; this is confirmed by the microstructure with fine recrystallized grains. The Thermo Mechanical Affected Zone (TMAZ) is also distinguished through optical microscopy. Fig. 7b represents the ‘nugget’ zone at a distance of 2 mm from the weld centre at the AA2024 side, which consists of fine and equiaxed grains. The higher temperatures and severe plastic deformations result in remarkable smaller grains compared to the base metal, according to all the FSW literature data for aluminium alloys; the initial elongated.

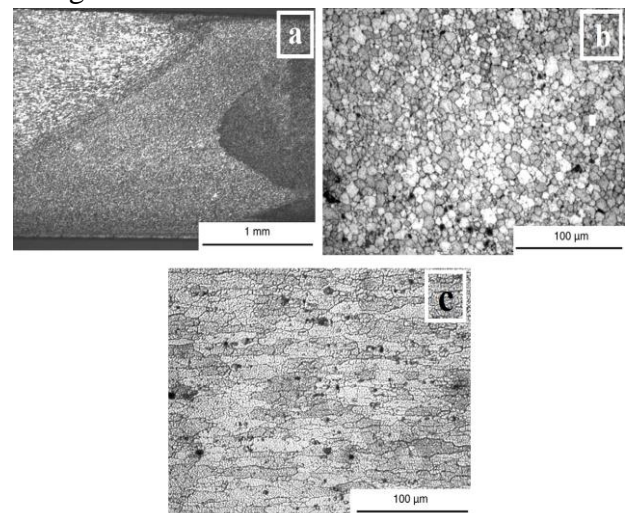


Fig. 7 Optical micrographs of FSW AA 2xxx and AA 7xxx aluminium alloys a) Cross

section of the welded specimen: particular of the nugget zone, TMAZ and base material interface, b) Fine recrystallized grains observed at a distance of 2 mm from the weld centre of the studied joints at the AA2024 side and c) Grains of parent material appearing at a distance of 4 mm from the weld centre of the joints at the AA7075 side.

Focusing away from the weld centre part at the AA7075 side, the grain dimension considerably increases and the orientation results with a less equiaxed character (Fig. 7c).

In particular, at a distance of 4 mm from the weld centre, a large amount of resident parent material grains start to appear. This region corresponds to the Heat Affected Zone, where the hardness is low with respect to the base metal. In fact, the precipitates in this area are coarsened as discussed. In the region adjacent to the nugget, i.e. TMAZ, no recrystallization apparently occurs because of the low temperature field originated by the Friction Stir process.

Vickers's micro hardness tests were conducted across the various regions of the weld spacing of (0.25mm) shown in Fig 8. Average hardness value of 105.15 HV was obtained across the weldment for cylindrical pin, and 135.6 HV.

The hardness of weld nugget was considerably lower than that of AA 2024; on the other hand, the hardness is comparatively higher than AA 7075 base material and TMAZ.

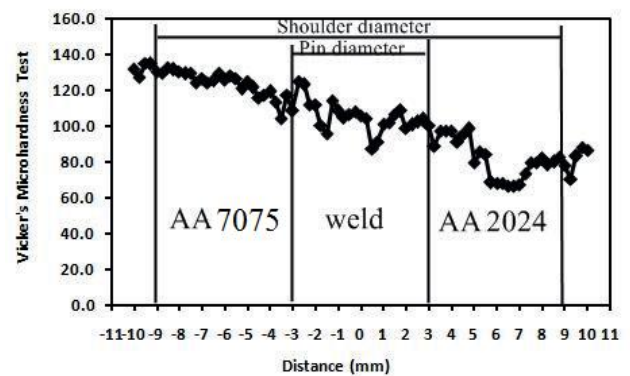


Fig. 8 Vicker's hardness tests were conducted across the various regions of the weld spacing

From the macro-graphic studies, different regions of weldments are identified and it represents the effective stir of both the base material in the nugget zone Fig 9. Also, the presence of AA2024 in the stirred zone is more when compared with AA7075, as the former was kept on the advancing side. Defect free welds were produced on using cylindrical pin with process parameter of 1100 rpm, 28 mm/min. Further it is supported by Balasubramanian et al. [6] where the author discussed the effect of tool pin profile with respect to weld property.

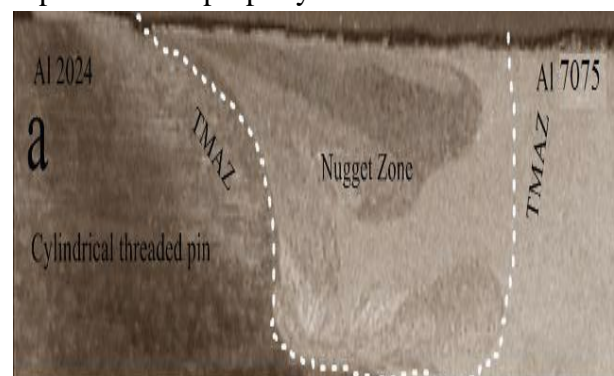


Fig. 9 Weld ability Macrostructure, a-cylindrical pin

3.5.1 Mechanical properties of FSW

The static response of all the AA2024 and AA7075 dissimilar sheets joined by friction

stir welding. The traction curves show a classical and remarkable behaviour; the mechanical properties, compared to the parent metals, are reported in Table 3. The joints exhibit very good ductile properties after yielding and the Ultimate Tensile Stress is settled at high levels. Even that the FS Welded specimens show lower proof stress at 0.2% and limited total elongations with respect to the base metals, the mechanical results are extremely good considering the drastic conditions to which the materials are subjected during the Friction Stirring process. All the tested specimens fractured beside the weld HAZ zones, close to the AA2024 and AA 7075 material side. This is in accordance with the behaviour of dissimilar welded sheets in which, from a microstructural point of view, the mechanical response of the centre weld results higher than the parent material and the HAZ because of the grain dimension differences and the precipitates concentration at the interfaces. In the lateral zones, in fact, the mean grain equivalent diameter resulted from the optical images to be around 5 μ m.

Table- 3 Mechanical Properties of AA2xxx and AA7xxx with FSW

Conditions	HV _(0.3)	Stress (MPa)	Strain (%e)
AA 2xxx	140	520±10	8
AA 7xxx	165	580±10	6
FSW	130	450±10	9

4. Under water FSW Processes Result and Discussion

Microstructural analysis

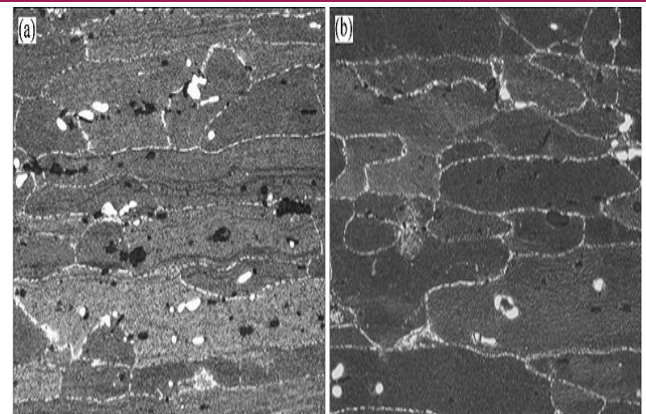


Fig. 10 SEM images of joints: (a) FSW, (b) Under water FSW

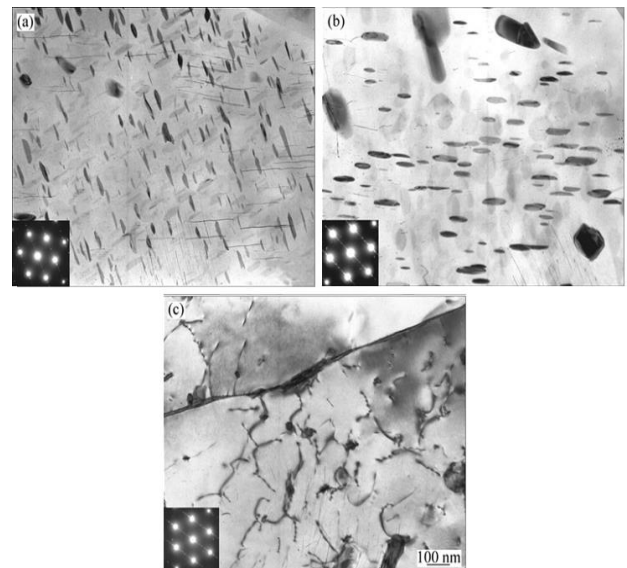


Fig. 11 TEM micrographs and selected area diffraction (SAD) patterns along [110]Al of aluminum matrix of precipitates in joints: (a) AA 7xxx; (b) AA 2xxx; (c) Underwater FSW joint

Micro hardness distributions

The micro-hardness distributions of the joints are shown in Fig. 12. It is clear that a soften region consisting of the WNZ, TMAZ and HAZ is created in both normal and underwater FSW joints, which is a typical characteristic for FSW of precipitate hardened aluminum alloys. For the normal joint, the hardness

profile shows a “W-type” and the minimum hardness (HV 78–81) is in the HAZ on the AS, corresponding to the fracture location of the joint. However, the hardness profile of the underwater joint exhibits quite different features. The soften region is remarkably narrowed, and the minimum hardness (HV 87–88) lies on the interface between WNZ and TMAZ on either side of the weld, which also coincides with the fracture location of the joint. The minimum hardness of the underwater joint is higher than that of the normal joint, thus the tensile strength of the underwater joint is improved. In further observation, it is found that the underwater joint has lower hardness in the WNZ and higher hardness in the TMAZ and HAZ, which is contrast to the normal joint. As for precipitate-hardened aluminum alloy, it has been widely reported that the hardness of the joint is synthetically controlled by precipitate distribution, dislocation density, grain size and solid solution which are all affected by external water cooling in the present study. Further microstructural analysis was carried out to reveal the tensile features of the joints.

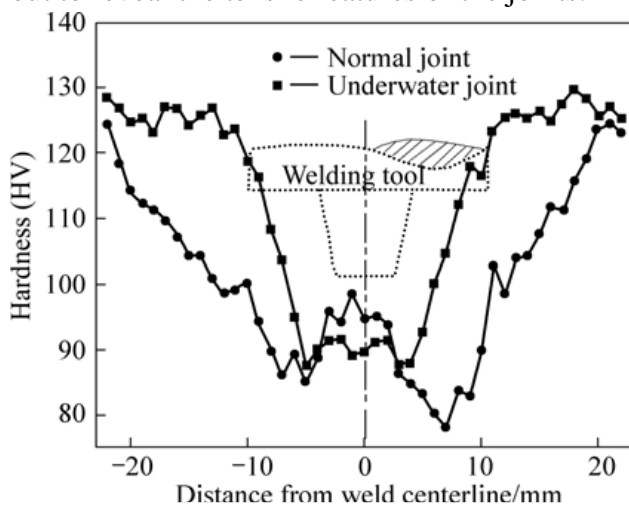


Fig. 12 Microhardness distributions of different joints

Tensile properties

The tensile properties of the joints are shown in Fig. 13 and the error bars are based on the standard deviation. The normal joint has a tensile strength of 324 MPa, equivalent to 75% that of the base metal. Through underwater FSW, joints with tensile strength of 341 MPa can be produced, approximately 79% that of the base metal which is comparable to the maximum tensile strength obtained in normal condition. Such a result indicates that the tensile strength of the joint can be improved by underwater FSW. However, the elongation of the underwater FSW joint only reaches 7.6% which is lower than that of the normal joint. The exact fracture locations of the joints are shown in Fig. 14 respectively. Normal and underwater RSW joints exhibit quite different fracture features. The tensile specimens of the normal joint fracture in the heat affected zone (HAZ) near the interface between the thermal mechanically affected zone (TMAZ) and HAZ on the AS (see Fig. 14(a)), implying that the HAZ is the intrinsic weakest location of the joints; while the tensile specimens of the underwater joint fracture at the interface between the weld nugget zone (WNZ) and TMAZ on the AS (see Fig. 4(b)), suggesting a strength improvement in the HAZ. Presents the fracture surfaces of normal and underwater FSW joints, which further confirms the plasticity difference between the two joints. The fracture surface of the normal FSW joint is characterized by large dimples (Fig. 14(a)), indicating that an extensive plastic deformation occurs during tensile test. However, dimple feature becomes ambiguous in the fracture surface of the underwater joint

(Fig. 14(b)), suggesting a decrease of plastic deformation level.

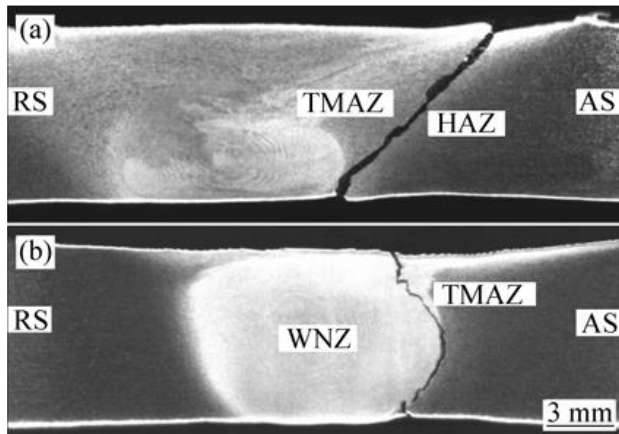


Fig. 13 Fracture locations of different joints:
(a) Normal FSW; (b) Underwater FSW

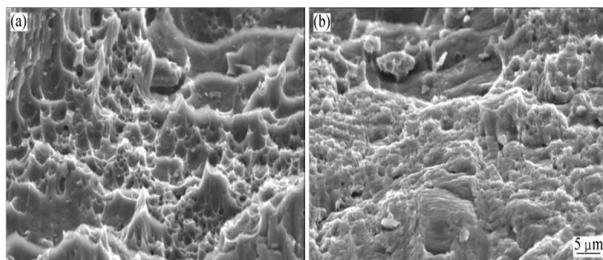


Fig. 14 Fracture surfaces of different joints:
(a) Normal FSW; (b) Underwater FSW

5. Conclusions

The dissimilar AA2024 and AA7075 aluminium alloys in the form of 6 mm thick sheets have been successfully joined by friction stir welding. The resulting microstructure has been widely investigated by optical microscopy, putting in evidence the grain structure and precipitates distribution differences originated by the process. Finally, the welded joints static and dynamic properties have been mechanically evaluated by means of tensile tests.

1) The tensile strength of the joint is improved, whereas the plasticity is deteriorated by underwater FSW.

2) The underwater FSW joint tends to fracture at the interface between WNZ and TMAZ on the AS during tensile test, while the normal joints fracture in the HAZ on the AS.

3) Compared with the normal FSW joint, the underwater FSW joint exhibits lower hardness in the WNZ and higher hardness in the TMAZ and HAZ.

6. References

- [1] W.M. Thomas, E.D. Nicholas, J.C. Needam, M.G. Murch, P. Templesmith, C.J. Dawes, GB Patent Application No. 9125978.8, December 1991 and US Patent No. 5460317, October 1995.
- [2] G. Bussu, P.E. Irving, The role of residual stress and heat affected zone properties on fatigue crack propagation in friction stir welded 2024-T351 aluminium joints, *International Journal of Fatigue* 25 (2018) 77–88.
- [3] K.V. Jata, K.K. Sankaran, J. Ruschau, Friction stir welding effects on microstructure and fatigue of aluminium alloy 7050 - T7451, *Metallurgical and Materials Transactions 31A* (2016) 2181–2192.
- [4] I. Charit, R.S. Mishra, M.W. Mahoney, Multi-sheet structures in 7475 aluminum by friction stir welding in concert with post-weld superplastic forming, *Scripta Materialia* 47 (2012) 631–636.
- [5] C.G. Rhodes, M.W. Mahoney, W.H. Bingel, M. Calabrese, Fine-grain evolution in friction-stir processed 7050 aluminium, *Scripta Materialia* 48 (2013) 1451–1455.
- [6] K.V. Jata, S.L. Semiatin, Continuous dynamic recrystallization during friction stir

welding of high strength aluminium alloys, *Scripta Materialia* 43 (8) (2010) 743–749.

[7] J.Q. Su, T.W. Nelson, R. Mishra, M. Mahoney, Microstructural investigation of friction stir welded 7050-T651 aluminium, *Acta Materialia* 51 (2013) 713–729.

[8] C.G. Rhodes, M.W. Mahoney, W.H. Bingel, Effects of friction stir welding on microstructure of 7075 aluminium, *Scripta Materialia* 36 (2017) 69–75.

[9] P. Ulysse, Three-dimensional modelling of the friction stir welding process, *International Journal of Machine Tools and Manufacture* 42 (2012) 1549–1557.

[10] J.Q. Su, T.W. Nelson, R. Mishra, M. Mahoney, Microstructural investigation of friction stir welded 7050-T651 aluminium, *Acta Materialia* 51 (2003) 713–729.

[11] C.G. Rhodes, M.W. Mahoney, W.H. Bingel, Effects of friction stir welding on microstructure of 7075 aluminium, *Scripta Materialia* 36 (1997) 69–75.

[12] P. Cavaliere, E. Cerri, L. Marzoli, J. Dos Santos, Friction stir welding of ceramic particle reinforced aluminium based metal matrix composites, *Applied Composite Materials* 11 (4) (2014) 247–258.

[13] Y.S. Sato, M. Urata, H. Kokawa, K. Ikeda, Hall-petch relationship in friction stir welds of equal channel angular-pressed aluminium alloys, *Materials Science and Engineering A354* (2013) 298–305.

[14] P.B. Berbon, W.H. Bingel, R.S. Mishra, C.C. Bampton, M.W. Mahoney, Friction stir processing: a tool to homogenize nanocomposites aluminium alloys, *Scripta Materialia* 44 (2001) 61–66.

[15] W.B. Lee, Y.M. Yeon, S.B. Jung, The improvement of mechanical properties of friction-stir-welded A356 Al alloy, *Materials*

Science and Engineering A355 (2003) 154–159.

[16] I. Shigematsu, Y.J. Kwon, K. Suzuki, T. Imai, N. Saito, Joining of 5083 and 6061 aluminum alloys by friction stir welding, *Journal of Materials Science Letters* 22 (2003) 353–356.

[17] W.-B. Lee, Y.-M. Yeon, S.-B. Jung, The joint properties of dissimilar formed Al alloys by friction stir welding according to the fixed location of materials, *Scripta Materialia* 49 (2003) 423–428.

[18] J.A. Wert, Microstructures of friction stir weld joints between an aluminium-base metal matrix composite and a monolithic aluminium alloy, *Scripta Materialia* 49 (2003) 607–612.

[19] A.E. Morabito, Analisi termomeccanica degli effetti termoelastici e dissipativi associati al comportamento a fatica della lega di alluminio 2024T3, PhD Thesis, Università di Lecce, 2003